Comparison of model predictive control strategies for a fluidized catalytic cracker

A.T. Boum[1][*], A.Latifi[2] and J.P.Corriou[3]

[1]*Universite de Douala, ENSET B.P 1872 Douala, Cameroun*
[2]*Universite de Lorraine, LRGP, UMR 3349, Nancy, F-54001, France*
[3]*Universite de Lorraine, LRGP, UMR 3349, Nancy, F-54001, France*
[*]*Corresponding author E-mail:boumat2002@yahoo.fr*

Abstract

A FCC model is used to compare five different Model Predictive Control (MPC) strategies. The FCC process is a complex petrochemical unit with catalyst recycling that makes its behaviour highly nonlinear. The FCC comprises a riser, a separator and a regenerator with important heat coupling due to the endothermic cracking reactions of gas oil in the riser and the exothermic combustion reactions in the regenerator. The riser and the regenerator exhibit fast and slow dynamics respectively. The temperatures at riser top and in the regenerator should be controlled by manipulation of catalyst and air flow rates. All these nonlinear and coupled characteristics render the multivariable control problem difficult and thus the FCC process constitutes a valuable benchmark for comparing control strategies. Here, the performances of Dynamic Matrix Control, Quadratic Dynamic Matrix Control, MPC control with penalty on the outputs, NonLinear MPC control, Observer Based MPC control are compared.

Keywords: multivariable control ;model predictive control ; fluidized catalytic cracker ; step response ; benchmark.

1. Introduction

Catalytic cracking has been used for more than seventy years [1, 2, 3] in petrochemical plants for conversion of heavy gas oil into high-value gasoline and lighter components. It is considered as the main unit in a refinery. Its major economic importance has fostered many technical developments and several versions of Fluidized Catalytic Cracking (FCC) units have been patented and installed, such as Exxon Model IV FCC [4], UOP type FCC [3], Kellog Orthoflow Model F FCC [5].

The simulation of FCCs is performed at many different levels of detail [6, 7, 8, 9, 10, 11, 12], either for the riser or the regenerator. Even CFD models describe the behaviour of the riser [13] or the regenerator. Generally, the riser model complexity depends only on the number of lumps used to describe the cracking kinetics. However, the regenerator model differs much more according to the studies. In some of them, the regenerator is modelled as a Continuously Stirred Tank Reactor (CSTR), whereas in other studies the two-phase model of Kunii-Levenspiel [14]. is used as the basis for describing the dense bed mainly composed of the bubbles and the emulsion phase with a high density of catalyst particles. Even, in this latter case, sometimes the bubbles are considered like the dense phase as a CSTR [15], sometimes as a plug flow system [9, 10].

Many researchers underline the nonstationary behavior of FCCs evidently due to the catalyst recycling which provokes an important heat coupling between the riser and the regenerator. Thus, some authors have signaled multiple steady states [16, 17, 18, 19] though it is not a general case. In our case, we did not find multiple steady states.

Because of its economic importance and the control difficulties encoutered due to its multivariable characteristics, large interactions, important nonlinearities and the presence of constraints, FCCs have been the subject of many control studies such as controllability analysis and control structure [20, 21], [12], [22], [23], model predictive control [24, 25, 26, 5, 27], nonlinear model predictive control [4, 28], PI observers [29]. Different control configurations are studied by these authors with various choices for inputs, outputs and their respective numbers. It remains that, owing to the complexity of the FCC dynamics, the multivariable characteristics and the presence of constraints, MPC is often considered as the reference control method.

On-line optimization with large economic benefits is also reported by [30, 31, 32].

In this work, multivariable control of an FCC process by several MPC strategies using two manipulated inputs and two controlled outputs is addressed. The present paper is organized as follows. Section 2 is related to the FCC description together with its constitutive units. Section 3 deals with the different model predictive control strategies followed by their respective simulation results. Finally, the conclusions of the paper are presented in Section 4.

2. FCC model

Basically, the FCC process is a complex petrochemical unit the role of which is to produce lighter components such as gasoline, diesel from gas oil by cracking reactions. These latter take place in the riser

by contact between vaporized gas oil and the fluidized rising catalyst on the surface of which coke, a reaction product and a poison for the catalyst, is deposited. The FCC process (Figure 1) comprises a riser, a separator and a regenerator with important heat coupling between the endothermic cracking reactions of gas oil in the riser and the exothermic combustion reactions of coke and oxygen in the regenerator. The riser and the regenerator are the main units which exhibit fast and slow dynamics respectively. One of the main features of FCCs is the catalyst recycle that makes its behaviour highly nonlinear.

Cracking reactions occurring in the riser reactor are highly complex due to the nature of feed oil and for that reason, they are modelled using lumps, i.e. groups of chemical components having close chemical properties, such as gasoline. The number of lumps involved in the models of the literature varies a lot and some models, especially those with a large number of lumps, do not provide the heats of reaction which are necessary for describing the energy balance in the riser. Among these cracking models, can be mentioned three lumps [33], four lumps [34, 35], five lumps [36], six lumps [37], seven lumps [38], eight lumps [39, 40], nine lumps [41], ten lumps [42], fourteen lumps [13, 43]. For control purposes, a large number of lumps is not necessary but the energy balance is of prime importance. The role of the regenerator is to regenerate the spent catalyst coming from the separator by allowing the combustion of the coke deposited on the catalyst [26, 44, 45, 46]. It is operated either in full or partial combustion. The regenerated catalyst is returned to the foot of the riser.
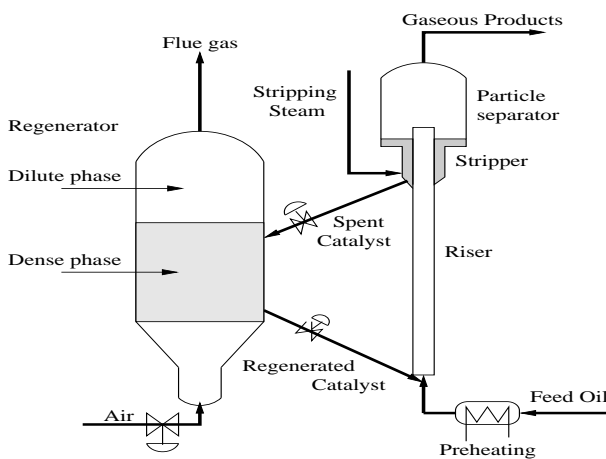
Figure 1: Schematic diagram of a FCC unit

2.1. Riser model

The riser is considered as a plug flow reactor. At the inlet, the feed is assumed to be instantaneously vaporized [12]. In the present model, it is assumed that no slip occurs between the solid phase and the gas phase, i.e. the velocities of both phases are equal. The residence time of catalyst and gas stream in the riser is supposed to be a few seconds. Consequently, the riser is only described by spatial equations and considered as an algebraic system with respect to time, opposite to the separator and regenerator whose equations are time-dependent. The kinetic model is based on a three-lump scheme [33] (Figure 2) to describe the cracking reactions in the riser [47]. The formation of coke is given by a simple algebraic equation at the outlet. In the literature, there exist many different models for the cracking in the riser, with lumps from three components up to fifteen components. Even if the number of components is particularly low in the present model, the main characteristics of the riser are taken into account such as the consumption of gas oil, the formation of gasoline and the endothermicity of the reaction with the decrease of temperature

along the riser.
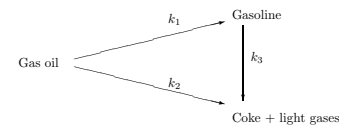
Figure 2: Three lump kinetics

In the riser model, a dimensionless spatial variable z is used, i.e. at bottom $z = 0$ and at top $z = 1$ corresponding to the actual height L. The feed temperature $T_{ris}(z = 0)$ at riser inlet results from the following heat balance

$$F_{cat,reg}C_{pcat}(T_{reg} - T_{ris,0}) = F_{feed}[C_{p,ol}(T_{boil} - T_{feed}) + \Delta H_{vap} + C_{p,og}(T_{ris,0} - T_{boil})]$$

that describes the heating of the liquid feed, its vaporization and finally the heating of the gas feed. $F_{cat,reg}$ is the catalyst flow rate from the regenerator. **Mass balance of gas oil**

$$\frac{dy_{go}}{dz} = -k_1 y_{go}^2 C_{owr} \phi t_c \tag{1}$$

where k_1 is the kinetic constant for gasoil consumption, C_{owr} is the ratio of catalyst flow rate to oil flow rate, y_{go} is the mass fraction of gasoil in the riser, t_c is the residence time of the catalyst in the riser. ϕ is the deactivation factor of the catalyst due to coke deposition. **Mass balance of gasoline**

$$\frac{dy_g}{dz} = (\alpha_2 k_1 y_{go}^2 - k_3 y_g) C_{owr} \phi t_c \tag{2}$$

where y_g is the mass fraction of gasoline. **Energy Balance**

$$\frac{dT_{ris}}{dz} = \frac{\Delta H_{crack}F_{feed}}{(F_{cat,reg}C_{pcat} + F_{feed}C_{po} + \lambda F_{feed}C_{p,steam})} \frac{dy_{go}}{dz} \tag{3}$$

where ΔH_{crack} is the heat of reaction and F_{feed} and $F_{cat,reg}$ are the respective flow rates of the gasoil and catalyst. The kinetic constants follow Arrhenius law. λ is the weight fraction of steam in the feed stream to the riser. The deactivation of the catalyst by the coke deposition is given as

$$\phi = (1 - mC_{coke,reg}) \exp(-\alpha t_c z C_{owr}) \tag{4}$$

Following [48], the produced coke concentration is empirically given by

$$C_{coke,prod} = k_c \sqrt{\frac{t_c}{C_{rc}^N} \exp(\frac{-E_{acf}}{R T_{ris,1}})} \tag{5}$$

where $T_{ris,1}$ is the temperature at the riser outlet. The amount of coke leaving the riser is given by

$$C_{coke,ris,1} = C_{coke,reg} + C_{coke,prod} \tag{6}$$

2.2. Separator model

The residence time of catalyst in the separator is frequently of the order of one minute. This separator can be modelled as a Continuously Stirred Tank Reactor (CSTR).
Mass balance of coke on catalyst

$$\frac{dC_{coke,sep}}{dt} = \frac{F_{cat,spent}(C_{coke,ris,1} - C_{coke,sep})}{m_{cat,sep}} \tag{7}$$

where $C_{coke,sep}$ is the coke concentration in the separator, $F_{cat,spent}$ is the flow rate of catalyst from the riser, $m_{cat,sep}$ is the catalyst holdup.
Energy balance

$$\frac{dT_{sep}}{dt} = \frac{C_{p,cat} F_{cat,spent}(T_{ris,1} - T_{sep})}{m_{cat,sep}C_{p,cat}} \tag{8}$$

where T_{sep} is the separator temperature.

2.3. Regenerator model

The regenerator model is inspired from [15]. The regenerator is a fluidized bed where air bubbles cross the dense bed formed by the catalyst. This bed is considered as a CSTR where the residence time of catalyst is frequently between ten and twenty minutes. The air bubbles through the bed could be modelled as a plug flow, however for ease of simulation, they are modelled as a CSTR. The temperature and amount of coke are considered uniform throughout the dense bed as well as the oxygen concentration. An important feature of the FCC is that the reactions in the riser are mainly endothermic whereas those in the regenerator are exothermic, thus the heat released in the regenerator is used by the riser by means of the transported catalyst. As the process involves a recycle, the behavior of a FCC is difficult to simulate correctly in both steady and transient states. In the FCC, partial combustion is assumed, i.e. carbon monoxide leaves the dense bed and is later oxidized to carbon doxide in the freeboard, not represented here. The model equations are derived from mass and energy balances.

Mass Balance of coke on the catalyst

$$\frac{dC_{coke,reg}}{dt} = \frac{(F_{cat,spent} C_{coke,sep} - F_{cat,reg} C_{coke,reg}) - \mathscr{R}_{cb}}{m_{cat,reg}} \quad (9)$$

where $C_{coke,reg}$ is the coke concentration on catalyst, $m_{cat,reg}$ is the catalyst inventory, $F_{cat,reg}$ is the catalyst flow rate leaving the regenerator. The rate of coke combustion is given by

$$\mathscr{R}_{cb} = k_{cb} \exp(-\frac{E_{acb}}{RT_{reg}}) x_{O2} C_{coke,reg} m_{cat,reg} \quad (10)$$

Energy balance

$$\frac{dT_{reg}}{dt} = \frac{1}{(m_{cat,reg} C_{p,cat})} [C_{p,cat}(F_{cat,spent} T_{sep} - F_{cat,reg} T_{reg})$$
$$F_{air,reg} C_{p,air}(T_{air} - T_{reg}) - \Delta H_{cb} \frac{\mathscr{R}_{cb}}{M_{w,coke}}] \quad (11)$$

where T_{reg} is the regenerator temperature, ΔH_{cb} is the enthalpy of coke combustion.

Mass balance of oxygen in the dense bed

$$\frac{dx_{O2}}{dt} = \frac{1}{m_{air,reg}} [\quad F_{air,reg}/M_{w,air}(x_{o2,in} - x_{o2,reg})$$
$$-((1+\sigma)n_{CH} + 2 + 4\sigma)/(4(1+\sigma))\mathscr{R}_{cb}/M_{w,coke}] \quad (12)$$

where σ is the molar ratio of CO_2 to CO in the dense bed, n_{CH} is the number of moles of hydrogen per mole of carbon in the coke.

The signification of parameters as well as their values for the FCC are given in Table 1. Typical steady-state values of the states and manipulated inputs are given in Table 2.

The code representing the FCC behaviour and all the Model Predictive Control codes were written in Fortran90. Efficient numerical and optimization routines were used [49], lsoda [50] for integration of differential equations, NLPQL [51] and BFGS [52] for nonlinear optimization. In the particular case of quadratic optimization, the only routines necessary for its solution were extracted from NLPQL code.

3. Comparison of Model Predictive Control Strategies

Several Model Predictive Control (MPC) strategies will be compared on the FCC process. Thus the simple model of the FCC can be considered as a valuable benchmark to perform a comparison of multivariable control schemes. The intention is not to provide the best control tuning for each control strategy, but rather to demonstrate how, by means of FCC model, it is possible to highlight the differences between different strategies and choices of control parameters. Table 3 shows the two manipulated inputs and the two controlled outputs of the FCC. Table 4 gives a brief summary of the different strategies which are compared in the present paper. All these strategies are very well detailed in [53, 54].

Table 1: FCC parameters, variables and initial data

Symbol	Meaning	Value
$C_{p,air}$	Heat capacity of air ($J.kg^{-1}.K^{-1}$)	1074
$C_{p,cat}$	Heat capacity of catalyst ($J.kg^{-1}.K^{-1}$)	1005
$C_{p,o}$	Heat capacity of liquid oil ($J.kg^{-1}.K^{-1}$)	2671
$C_{p,steam}$	Heat capacity of steam ($J.kg^{-1}.K^{-1}$)	1900
E_{acf}	Activation energy for coke formation ($J.mol^{-1}$)	$20\ 10^3$
E_{a1}	Activation energy for cracking of gas oil (feed) ($J.mol^{-1}$)	$101.5\ 10^3$
E_{a3}	Activation energy for cracking of gasoline ($J.mol^{-1}$)	$112.6\ 10^3$
$F_{air,reg}$	Mass flow rate of air to regenerator ($kg.s^{-1}$)	25.378
$F_{cat,reg}$	Mass flowrate of catalyst ($kg.s^{-1}$)	294
F_{feed}	Mass flow rate of feed ($kg.s^{-1}$)	40.63
k_c	Reaction rate constant for catalytic coke formation ($s^{-0.5}$)	0.0093
$k_{1,0}$	Reaction rate constant for the total rate of cracking of gas oil	$9.65\ 10^5$
$k_{3,0}$	Reaction rate constant for the total rate of cracking of gas oil	$4.22\ 10^5$
m	Empirical deactivation parameter	80
$m_{air,reg}$	Holdup of air in the regenerator (mol)	20000
$m_{cat,reg}$	Holdup of catalyst in regenerator (kg)	175738
$m_{cat,sep}$	Holdup of catalyst in separator (kg)	17500
$M_{w,coke}$	Molecular weight of coke ($kg.mol^{-1}$)	$14\ 10^{-3}$
n_{CH}	Number of moles of hydrogen per mole of carbon in the coke	2
T_{air}	Temperature of air to regenerator (K)	360
T_{boil}	Boiling temperature of the feed (K)	700
t_c	Residence time in the riser (s)	9.6
T_{feed}	Feed temperature (K)	434.63
α	Catalyst decay rate constant (s^{-1})	0.12
α_2	Fraction of gas oil which cracks to gasoline	0.75
ΔH_{vap}	Heat of feed vaporization ($J.kg^{-1}$)	$1.56\ 10^5$
ΔH_{crack}	Heat of cracking ($J.kg^{-1}$)	$506.2\ 10^3$
λ	Weight fraction of steam in feed stream to riser	0.035
σ	Molar ratio of CO_2 to CO in the dense bed	

Table 2: FCC steady-state values of the states for $F_{air,reg} = 25.571 kg.s^{-1}$ and $F_{cat,reg} = 295.03 kg.s^{-1}$ at a given temperature set point

Symbol	Meaning	Value
$C_{coke,ris,1}$	Coke concentration at top of riser (kg coke/kg cat)	0.00974
$C_{coke,reg}$	Coke concentration in the regenerator (kg coke/kg cat)	0.00305
$T_{ris,0}$	Temperature in the riser at inlet (K)	805.70
$T_{ris,1}$	Temperature in the riser at top of riser (K)	780.00
T_{sep}	Temperature in the separator (K)	780.00
T_{reg}	Temperature in the regenerator (K)	972.00
x_{O2}	Oxygen mole fraction in regenerator	0.00591
y_{go}	Mass fraction of gas oil at top of riser	0.458
y_g	Mass fraction of gasoline at top of riser	0.383

Table 3: Manipulated inputs and controlled outputs

Manipulated input u_1	Mass flow rate of catalyst $F_{cat,reg}$
Manipulated input u_2	Mass flow rate of air $F_{air,reg}$
Controlled output y_1	Temperature at top of riser $T_{ris,1}$
Controlled output y_2	Temperature in the regenerator T_{reg}

3.1. Identification by open loop responses

In many cases, open loop responses of the system are necessary to identify a model of the system which is later used for closed loop control. The sampling period is taken equal to 250s. In all cases, the model horizon was equal to 60 sampling time. In several of the MPC strategies (DMC, QDMC, MPC-penalty), the linear model of the

Table 4: Summary of control strategies

Control strategy (Symbol) Basis (Type of optimization)
Dynamic Matrix Control (DMC)
Linear model using step response coefficients,
without constraints
(analytical solution)
Quadratic Dynamic Matrix Control (QDMC)
Linear model using step response coefficients,
with hard constraints on u and Δu
(quadratic programming)
Model Predictive Control (MPC-penalty)
Linear model using step response coefficients,
with hard constraints on u, Δu and soft constraints on y
(nonlinear optimization with penalty function)
NonLinear Model Predictive Control (NLMPC)
Nonlinear model of the process, with hard constraints on u, Δu
(nonlinear optimization)
Observer Based Model Predictive Control (OBMPC)
State-space linear model using step response coefficients,
with hard constraints on u, Δu,
Kalman filter
(quadratic programming)

process is given by the dynamic matrix from equation (18) formed by the unit step response coefficients of the studied controlled outputs with respect to all the manipulated inputs. Even, OBMPC uses this information, but in a different way. Thus, step variations of mass flow rate of catalyst (5%) and mass flow rate of air (0.5%) are imposed to the process around a steady state (Figure 3). The responses of the controlled outputs with respect to the mass flow rate of catalyst are shown in Figure 4 as they are particularly interesting. The normalized time is indicated in numbers of sampling periods. When the step on u_1 is imposed at normalized time 81, immediately the temperature at the top of the riser increases abruptly. This is due to the algebraic character of the riser model equations, i.e. its dynamics is neglected with respect to that of the rest of the system. After that, the riser temperature decreases and then increases, thus showing an inverse response characteristics. The first decrease is due to the fact that the endothermic heat of reaction overcomes the sensible heat brought by the catalyst, but later the regenerator temperature will increase and finally cause increase of bottom riser temperature and consequently top riser temperature. The regenerator temperature is influenced by the riser temperature and will vary in a relatively similar way to the step of mass flow rate of catalyst. The responses of the top riser temperature and regenerator temperature to steps of mass flow rate of air are simpler and close to first order responses. Of course, the step response coefficients (Figures 5 and 6) display the same dynamical tendencies that were previously described.
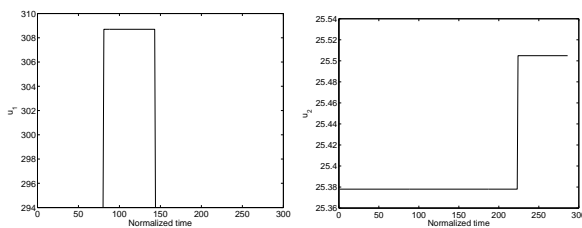
Figure 3: Mass flow rate of catalyst and mass flow rate of air imposed for open loop identification
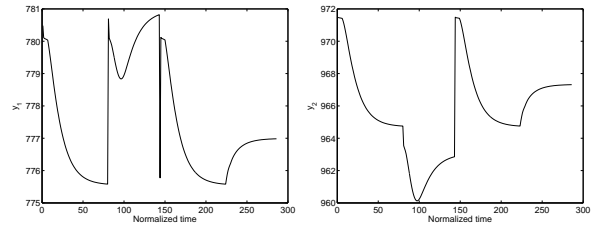
Figure 4: Responses of top riser temperature and regenerator temperature used for open loop identification
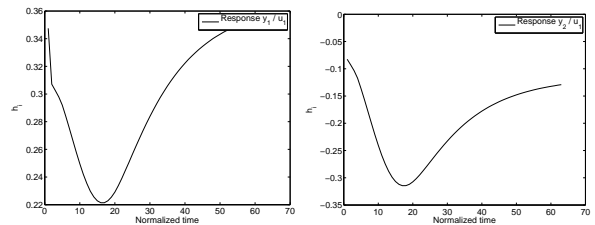
Figure 5: Unit step response coefficients for both outputs with respect to manipulated mass flow rate of catalyst
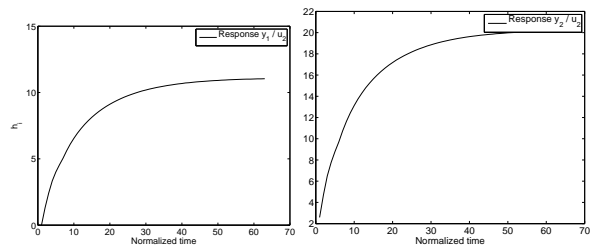
Figure 6: Unit step response coefficients for both outputs with respect to manipulated mass flow rate of air

3.2. Dynamic Matrix Control

3.2.1. General presentation

To simplify the presentation, DMC is first presented in a SISO framework [55, 56, 53, 54]. At time k, the following quadratic criterion taking into account the differences between the estimated outputs $\hat{y}(k+i|k)$ and the references on the prediction horizon H_p

$$J = \sum_{i=1}^{H_p} (\hat{y}(k+i|k) - y^{ref}(k+i))^2 \tag{13}$$

is minimized, in the absence of constraints, with respect to the variations of $\Delta u(k)$ of the manipulated input considered over a control horizon H_c.

The plant is represented by a stable step reponse, i.e. the step response coefficients. The prediction of the ouput based on past and future inputs is given by

$$\hat{y}(k+l|k) = y_{ss} + \sum_{i=l+1}^{H_m-1} h_i \Delta u(k+l-i) + h_M (u(k+l-M) - u_{ss})$$

$$\sum_{i=1}^{l} h_i \Delta u(k+l-i) + \hat{d}(k+l|k) \tag{14}$$

where h_M is the model horizon which must be larger than or equal to the prediction horizon H_p. The influence of unmodelled dynamics and disturbances is globally taken into account by the disturbance term

$$d(k) = y(k) - y^*(k|k) \tag{15}$$

Given the measured output $y^m(k)$, the future disturbances are estimated as

$$\hat{d}(k+l|k) = \hat{d}(k|k) = y^m(k) - y^*(k|k) \qquad (16)$$

i.e. all the future predicted disturbances are equal to the present disturbance estimation.

The output prediction based on past inputs is defined as

$$y^*(k+l|k) = y_{ss} + \sum_{i=l+1}^{M-1} h_i \Delta u(k+l-i) + h_M(u(k-1) - u_{ss}) \qquad (17)$$

The vector of output predictions $\hat{y}(k+l|k)$ is related to the vector of ouput predictions $y^*(k+l|k)$ based on past inputs, to the vector of inputs $\Delta u(k)$ and to the vector of predicted disturbances as

$$\begin{bmatrix} \hat{y}(k+1|k) \\ \vdots \\ \hat{y}(k+H_p|k) \end{bmatrix} = \begin{bmatrix} y^*(k+1|k) \\ \vdots \\ y^*(k+H_p|k) \end{bmatrix} + \mathscr{A} \begin{bmatrix} \Delta u(k) \\ \vdots \\ \Delta u(k+H_c-1) \end{bmatrix} + \begin{bmatrix} \hat{d}(k+1|k) \\ \vdots \\ \hat{d}(k+H_p|k) \end{bmatrix}$$

where $\mathscr{A}$ is the dynamic matrix made of step response coefficients h_i of the plant outputs to the manipulated inputs.

$$\mathscr{A} = \begin{bmatrix} h_1 & 0 & \dots 0 \\ h_2 & h_1 & \vdots \\ \vdots & \vdots & \ddots \\ h_M & h_{H_c-1} & \dots h_1 \\ \vdots & \vdots & \vdots \\ h_M & h_{M-1} & \dots & h_{M-H_c+1} \\ \vdots & \vdots & \vdots \\ h_M & h_M & \dots h_M \\ \vdots & \vdots & \vdots \\ h_M & h_M & \dots h_M \end{bmatrix} \qquad (18)$$

For a multivariable system of dimension $n_u \times n_y$, the dynamic matrix is simply composed of submatrices as

$$\mathscr{A} = \begin{bmatrix} \mathscr{A}_{11} & \dots & \mathscr{A}_{1n_u} \\ \vdots & & \vdots \\ \mathscr{A}_{n_y 1} & \dots & \mathscr{A}_{n_y n_u} \end{bmatrix} \qquad (19)$$

According to past equations, the vector of future input moves is given as

$$\Delta u(k) = [\Delta u_1(k)^T \dots \Delta u_{n_u}(k)^T]^T \qquad (20)$$

which is the least-squares solution of the following linear system

$$\begin{bmatrix} y^{ref}(k+1) - y^*(k+1|k) - \hat{d}(k|k) = e(k+1) \\ \vdots \\ y^{ref}(k+H_p) - y^*(k+H_p|k) - \hat{d}(k|k) = e(k+H_p) \end{bmatrix} = e(k+1) = \mathscr{A}\Delta u(k)$$

$$(21)$$

In the absence of constraints, the least-squares solution is

$$\Delta u(k) = (\mathscr{A}^T \mathscr{A})^{-1} \mathscr{A}^T e(k+1) \qquad (22)$$

Only the first component of $u(k)$ is implemented at time k.
In fact, the modified criterion (24) of QDMC will be used even for DMC to rigorously use the same criterion.
The different MPC strategies which are presented were developed in Fortran90 and they can be applied for a stable system having any number of inputs and outputs. The values of the main parameters which influence the studied MPC strategies are given in Table 5.

3.2.2. Numerical results

In the open loop responses, it has been observed that when a step on the catalyst flow rate was imposed, the outputs exhibited an inverse response behaviour. It will be shown in the following that it has important consequences. The inverse response is even more difficult to handle than a pure delay to which it could be compared. For that reason, a modified criterion with a lower $H_{p,low}$ bound of the prediction horizon which can be varied is implemented as

$$J = \sum_{i=H_{p,low}}^{H_p} (\hat{y}(k+i|k) - y^{ref}(k+i))^2 \qquad (23)$$

The lower bound is used in MPC to avoid problems arising from the inverse response of processes and in our case we have a case of an inverse response. The set points have been chosen as positive and negative steps occurring at different times to emphasize the interaction effects that can influence the closed loop control of such a process. Thus, with respect to the steady state, the set point of the riser temperature undergoes an increase of 5K at $t = 20000$s and a decrease of 5K at $t = 40000$s whereas the set point of the regenerator temperature undergoes an increase of 5K at $t = 60000$s and a decrease of 5K at $t = 80000$s, the total simulation time being equal to 100000s.

DMC case with $H_{p,low} = 1$.
The first choice of parameters was $H_p = 20$, $H_{p,low} = 1$, $H_c = 3$. When the original criterion (13) is used (Figures 7 and 8), i.e. with $H_{p,low} = 1$, strong oscillations of the riser temperature are visible at each set point change corresponding to strong oscillations of the catalyst flow rate and also sharp variations of the air flow rate. The oscillations are due to the inverse response behaviour of the temperatures to variations of the catalyst flow rate. The set points are well tracked for the riser and regenerator temperatures.
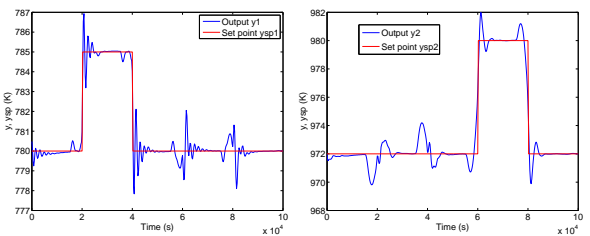
Figure 7: DMC control with $H_{p,low} = 1$. Left: Riser temperature (K). Right: Regenerator temperature (K).
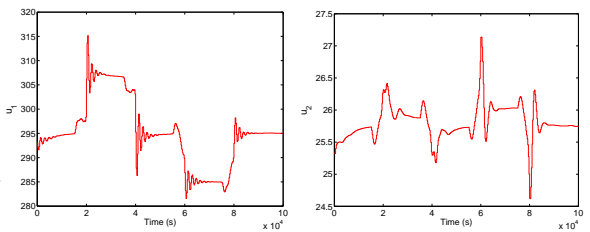
Figure 8: DMC control with $H_{p,low} = 1$. Left: Catalyst flow rate (kg/s). Right: Air flow rate (kg/s).

DMC case with $H_{p,low} = 10$.
To avoid the oscillations visible with $H_{p,low} = 1$, a larger value of $H_{p,low}$ equal to 10 is considered. It must be noticed that the duration of the inverse response (Figure 4) is about 15 sampling periods so that the value of $H_{p,low}$ is close to that duration. In these conditions, compared to the previous case where $H_{p,low} = 1$, the behaviour of the closed loop system is much improved with a smoother tracking of the set points (Figure 9). However, the interaction effects are

Table 5: Conditions of Model Predictive Control Strategies

Dynamic Matrix Control, first case	
Prediction horizon H_p	20
Lower bound of prediction horizon $H_{p,low}$	1
Control horizon H_c	3
Dynamic Matrix Control, second case	
Prediction horizon H_p	20
Lower bound of prediction horizon $H_{p,low}$	10
Control horizon H_c	3
Quadratic Dynamic Matrix Control	
Prediction horizon H_p	20
Lower bound of prediction horizon $H_{p,low}$	10
Control horizon H_c	3
Model Predictive Control with nonlinear optimization by NLPQL	
Prediction horizon H_p	20
Lower bound of prediction horizon $H_{p,low}$	1
Control horizon H_c	3
Nonlinear Model Predictive Control	
Prediction horizon H_p	3
Lower bound of prediction horizon $H_{p,low}$	1
Control horizon H_c	1
Observer Based Model Predictive Control, first case	
Measurement standard deviation σ_y	0.5
Prediction horizon H_p	3
Lower bound of prediction horizon $H_{p,low}$	1
Control horizon H_c	1
Observer Based Model Predictive Control, second case	
Measurement standard deviation σ_y	0.01
Prediction horizon H_p	3
Lower bound of prediction horizon $H_{p,low}$	1
Control horizon H_c	1

increased, for example on the riser temperature, around $t = 60000$s and $t = 80000$s. The profiles of the manipulated inputs are also different with smoother variations (compare Figures 8 and 10). Other sets of parameters $H_{p,low}$, H_p and H_c could have been chosen, but we recall that our objective is to show the potential of this FCC model for demonstrating the differences between various MPC strategies.
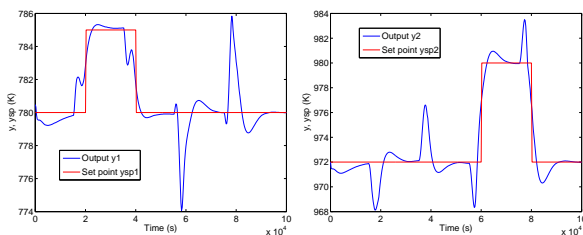
Figure 9: DMC control with $H_{p,low} = 10$. Left: Riser temperature (K). Right: Regenerator temperature (K).
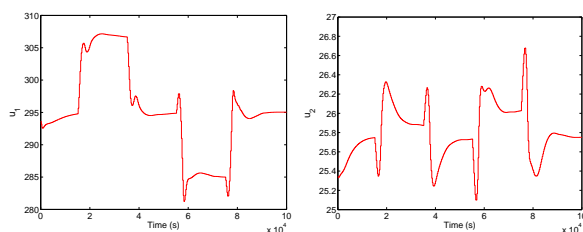
Figure 10: DMC control with $H_{p,low} = 10$. Left: Catalyst flow rate (kg/s). Right: Air flow rate (kg/s).

3.3. Quadratic Dynamic Matrix Control

In order to take into account the constraints, quadratic dynamic matrix control (QDMC) is used instead of DMC. Furthermore, a modification of the quadratic criterion as the sum of a performance term and an energy term is introduced in QDMC [56] as

$$J = \sum_{i=H_{p,low}}^{H_p} \gamma_i^2 (\hat{y}(k+i|k) - y^{ref}(k+i))^2 + \sum_{i=1}^{H_c} \lambda_i^2 (\Delta u(k+i))^2 \quad (24)$$

where the weights γ_i for the outputs are the elements of a diagonal matrix Γ, and the weights λ_i for the inputs are the elements of a diagonal matrix Λ. Hard constraints with respect to the manipulated variables and their moves are taken into account

$$\begin{aligned} u_{min} \leq u \leq u_{max} \\ \Delta u_{min} \leq \Delta u \leq \Delta u_{max} \end{aligned} \quad (25)$$

These constraints can be gathered as a system of linear inequalities incorporating the dynamic information concerning the projection of constraints [57]

$$B \Delta u(k) \leq c(k+1) \quad (26)$$

where B is a matrix and c a vector.

In the presence of constraints (25), the QDMC problem can be formulated as a quadratic programming problem [51] such as

$$\min_{\Delta u(k)} \left[\frac{1}{2} \Delta u(k)^T H \Delta u(k) - g(k+1)^T \Delta u(k) \right] \quad (27)$$

subject to constraints (25). H is the Hessian matrix which is equal to

$$H = \mathscr{A}^T \Gamma^T \Gamma \mathscr{A} + \Lambda^T \Lambda \quad (28)$$

where $\mathscr{A}$ is the dynamic matrix, g is the gradient vector equal to

$$g(k+1) = \mathscr{A}^T \Gamma^T \Gamma e(k+1) \quad (29)$$

In all cases, the weights Γ and Λ were diagonal matrices with respective values equal to 10 and 1, putting more weight on the controlled outputs. The constraints on u were chosen in such a way that they were never reached and no constraints on Δu were considered. The choice of parameters $H_p = 20$, $H_{plow} = 10$, $H_c = 3$, resulted in the same results as DMC with the same set of parameters. For that reason, the Figures are not shown. This is due to the absence of constraints so that the problems are exactly of the same nature and the numerical solution by optimizer NLPQL obtained for QDMC is the same as the analytical solution as DMC provided the same criterion (24) is minimized.

3.4. Model Predictive Control with nonlinear optimization by NLPQL

When soft constraints on the controlled outputs y are considered, the nature of the optimization problem changes with respect to QDMC. These soft constraints are taken into account by addition of a penalty term to the quadratic criterion (24) used in QDMC. To be able to compare with DMC and QDMC, the soft constraints on y were taken large so that they were never reached, making the penalty term equal to zero. In spite of this, the code was required to perform the nonlinear optimization as if soft constraints were present. Thus, the control problem results in a general problem of nonlinear optimization which is solved by NLQPL optimizer [51]. The same values of prediction horizon $H_p = 20$ and control horizon $H_c = 3$ were taken. However, between the two values of $H_{p,low}$ equal to 1 and 10, the value $H_{p,low} = 1$ gave much better results which are presented in Figures 11 and 12. This $H_{p,low} = 1$ is due to the difficulty of the

nonlinear optimization for the FCC. The set point tracking is excellent and the interaction effects at the set point changes are relatively small. The difference between these results and those of QDMC may be explained by the numerical approximations of the Lagrangian function and its gradient that are performed during the nonlinear minimization by a quasi-Newton method and which would result in a filtering and smoothing of the oscillations previously present in QDMC
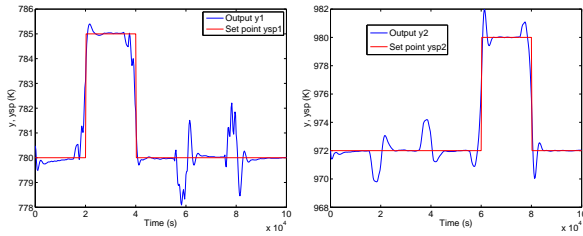
Figure 11: MPC control with nonlinear optimization by NLPQL and $H_{p,low} = 1$. Left: Riser temperature (K). Right: Regenerator temperature (K).
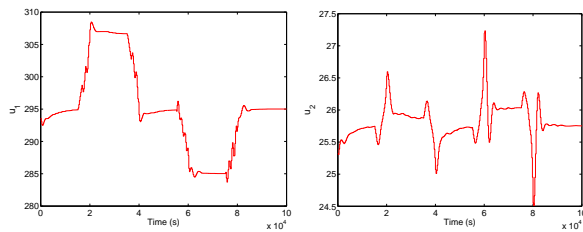
Figure 12: MPC control with nonlinear optimization by NLPQL and $H_{p,low} = 1$. Left: Catalyst flow rate (kg/s). Right: Air flow rate (kg/s).

3.5. Nonlinear Model Predictive Control with prediction from the nonlinear model described by ordinary differential equations

Nonlinear Model Predictive Control exists under several different forms [53, 58]. In particular, it can be performed by local linearization of the nonlinear state space model [59, 60] at each sampling instant. In the three previously described versions of MPC (DMC, QDMC, MPC with penalty on y), the outputs were predicted using the linear model based on the step response coefficients. In the nonlinear MPC described in this section, the nonlinear model

$$\dot{x} = f(x, u)$$
$$y = h(x) \tag{30}$$

constituted by the equations of the riser, the separator and the regenerator, is directly used to obtain the predicted states and consequently the predicted outputs as follows. At each sampling instant k, the nonlinear model (30) is integrated from k until $k + H_p$, i.e. over the prediction horizon by the integrator lsoda [50] well suited to stiff systems. From the calculated values of the states $x(k+i)$, $1 \leq i \leq H_p$, considered as the predicted states $\hat{x}(k+i)$, the predicted outputs $\hat{y}(k+i)$ are deduced. They are directly used in the calculation of the same criterion (24) as QDMC, but now the criterion depends in a nonlinear way on the manipulated inputs, opposite to the two first MPC control strategies (DMC, QDMC). Consequently, the optimization to be performed with respect to the future variations of the manipulated inputs $\Delta u(k+i)$ is nonlinear. Thus, the NLPQL optimizer [51] and BFGS routine [52] are used in the Fortran90 code to perform the nonlinear optimization. In the optimization process, it appears that it is more difficult to achieve a successful optimization at each sampling instant than in the other cases. This may be due to the highly nonlinear character of the FCC. Thus, the

large value of the prediction horizon $H_p = 20$ resulted in a failure of optimization. Considering $H_p = 20$ and $H_{p,low} = 10$ was no more successful. The best choices which were found corresponded to small values of prediction horizon H_p and very small control horizon H_c, typically $H_p = 3$ and $H_c = 1$. Moreover, at each sampling instant k, to find the optimum solution with respect to the manipulated input variations, the optimizer calculates the criterion a large number of times until some tolerance is reached, and for each calculation of the criterion, the nonlinear equations must be integrated. This resulted in a very long computation time which would not be adapted for on-line optimization and control. An important drawback of such a nonlinear optimization problem to be solved for control and on-line implementation is that it is required to guarantee successful optimization at each sampling instant. Other forms of nonlinear control are presented in the literature such as by [59, 60], but the local linearization which is proposed by these latter authors make it closer to linear MPC than real Nonlinear MPC.

Figure 13 shows that the regulation and tracking are well performed, but that the way to reach the setpoints and the interactions shows significant improvement with respect to the linear MPC strategies as the outputs exhibit lower deviations with respect to their respective set points around the set point changes. Figure 14 shows that, in general the variations of the manipulated inputs are smooth, especially the flow rate of catalyst. However, the set point tracking is less satisfactory.
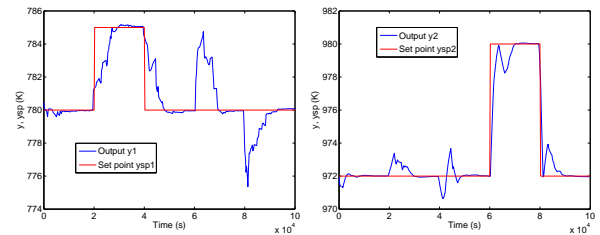
Figure 13: Nonlinear MPC control with $H_p = 3$, $H_c = 1$. Left: Riser temperature (K). Right: Regenerator temperature (K).
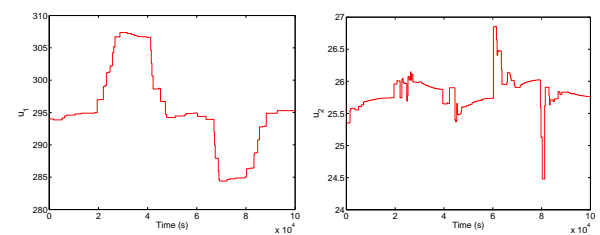
Figure 14: Nonlinear MPC control with $H_p = 3$, $H_c = 1$. Left: Catalyst flow rate (kg/s). Right: Air flow rate (kg/s).

3.6. Observer Based Model Predictive Control

3.6.1. General presentation

Many state-space approaches exist for MPC. They were first developed for linear MPC [61, 62, 63] and some of them have been later extended to nonlinear MPC [58]. As well as for DMC and QDMC, a predictor of the output is first built, then a state observer is developed to estimate the states. This observer-based model predictive control (OBMPC) developed by [61, 62], is briefly presented [49, 54] in the following.

A fundamental idea [64] is to represent the entire trajectory for a

SISO system as a sequence of states

$$x_1(k) = x_2(k-1) + h_1 \Delta u(k-1)$$
$$\vdots \tag{31}$$
$$x_i(k) = x_{i+1}(k-1) + h_i \Delta u(k-1), \qquad i = 1, M$$

where h_i are the step response coefficients. These equations are then used to obtain the predicted output corresponding to the influence of past variations

$$y^*(k+i-1|k) = y^*(k+i-1|k-1) + h_i \Delta u(k-1) \tag{32}$$

In the case of a MIMO system with n_u inputs and n_y outputs, the matrix S_k is defined at each instant k

$$S_k = \begin{bmatrix} h_{1,1,k} & h_{1,2,k} & \dots & h_{1,n_u,k} \\ h_{2,1,k} & h_{2,2,k} & \dots & h_{2,n_u,k} \\ \vdots & \vdots & \dots & \vdots \\ h_{n_y,1,k} & h_{n_y,2,k} & \dots & h_{n_y,n_u,k} \end{bmatrix} \tag{33}$$

where $h_{j,i,k}$ is the step coefficient at instant k of output j with step input i.

At time k, the future control actions $\Delta u(k+l)$ are to be determined over the control horizon.

In the absence of disturbances, the state-space form corresponding to the step response model can then be written as

$$\begin{aligned} Y(k) &= \Phi Y(k-1) + S \Delta u(k-1) \\ y^*(k|k) &= \Psi Y(k) \end{aligned} \tag{34}$$

with

$$Y(k) = [y^*(k|k)^T \ y^*(k+1|k)^T \ \dots y^*(k+M-1|k)^T \ x_u(k)^T \ x_w(k)^T]^T$$
$$y^*(k+i|k) = [y_1^*(k+i|k) \dots y_{n_y}^*(k+i|k)]^T$$
$$\Delta u(k) = [\Delta u_1(k) \dots \Delta u_{n_u}(k)]^T$$
$$\tag{35}$$

Similarly to the the LQG state-space model, the state-space model (34) can be extended [62] to take into account disturbances w and output noise v as

$$\begin{aligned} Y(k) &= \Phi Y(k-1) + S \Delta u(k-1) + T \Delta w(k-1) \\ y(k) &= y^*(k|k) + v(k) \\ y^*(k|k) &= \Psi Y(k) \end{aligned} \tag{36}$$

with the matrix Φ equal to

$$\Phi = \begin{bmatrix} 0 & I_{n_y} & 0 & \dots & 0 & 0 & 0 \\ 0 & 0 & I_{n_y} & \ddots & 0 & \vdots & \vdots \\ \vdots & \vdots & & \ddots & & \dots & \\ 0 & 0 & \dots & & I_{n_y} & 0 & 0 \\ 0 & 0 & \dots & & I_{n_y} & C_u & C_w \\ 0 & 0 & \dots & & 0 & A_u & 0 \\ 0 & 0 & \dots & & 0 & 0 & A_w \end{bmatrix} \tag{37}$$

the matrix S equal to

$$S = \begin{bmatrix} S_1 & \dots & S_M & B_u & 0 \end{bmatrix}^T \tag{38}$$

the matrix Ψ equal to

$$\Psi = \begin{bmatrix} I_{n_y} & 0 & \dots & 0 \end{bmatrix} \tag{39}$$

and the matrix T equal to

$$T = \begin{bmatrix} 0 & 0 & \dots & B_w \end{bmatrix}^T \tag{40}$$

Residual plant dynamics and disturbance dynamics are considered under a state-space form using matrices A_u, A_w, B_u, B_w, and C_u, C_w [54, 62].

The future outputs are predicted by means of a state observer such as the optimal linear Kalman filter of matrix gain K, operating in two stages, first, the model prediction

$$\hat{Y}(k+1|k) = \Phi \hat{Y}(k|k) + S \Delta u(k) \tag{41}$$

then, the correction based on measurements

$$\hat{Y}(k|k) = \hat{Y}(k|k-1) + K[y(k) - \hat{y}^*(k|k-1)] \tag{42}$$

with

$$\begin{aligned} \hat{Y}(k|k-1) &= [\hat{y}^*(k|k-1)^T \ \hat{y}^*(k+1|k-1)^T \ \dots \hat{y}^*(k+M-1|k)^T \\ &\quad \hat{x}_u \ \hat{x}_w]^T \\ \hat{y}^*(k|k-1) &= \Psi \hat{Y}(k|k) \end{aligned} \tag{43}$$

After state estimation, the optimization is performed as a quadratic programming problem like QDMC [56]. The objective function to be minimized with respect to $\Delta \mathscr{U}(k)$ is

$$J = \| \Gamma [\mathscr{Y}(k+1|k) - \mathscr{R}(k+1|k)] \|^2 + \| \Lambda \Delta \mathscr{U}(k|k) \|^2 \tag{44}$$

In the absence of constraints, the least-squares solution of OBMPC expressed by criterion (44) is

$$\Delta \mathscr{U}(k|k) = [\mathscr{S}_{H_p}^T \Gamma^T \Gamma \mathscr{S}_{H_p} + \Lambda^T \Lambda]^{-1} \mathscr{S}_{H_p}^T \Gamma^T \Gamma [\mathscr{R}(k+1|k) - \Phi_{H_p} \hat{Y}(k|k)] \tag{45}$$

where $\mathscr{S}_{H_p}$ is composed of matrices S_i [54, 62].

Thus, opposite to DMC, OBMPC uses an optimal state observer, the Kalman filter, for the predictor part. According to [62], the different decomposition of OBMPC as a predictor-optimizer avoids limitations of DMC-type algorithms, such as excessive number of step response coefficients, poor behaviour when submitted to ramp-like disturbances or in presence of strong interactions and the necessary stable behaviour of the plant.

3.6.2. Numerical results

The general parameters were always $H_p = 20$, $H_{p,low} = 10$, $H_c = 1$, as they gave very satisfactory results for tracking and regulation.

OBMPC with $\sigma_y = 0.01$

The case where the standard deviation $\sigma_y = 0.01$, i.e. close to zero, for both measured outputs, is first considered to compare this strategy based on a state space approach with the strategies based on step responses such as QDMC. In Figures 15 and 16, the set points are very well tracked, the multivariable interactions are much less important than with DMC and QDMC, the manipulated inputs vary very smoothly. Thus, globally the control is well improved.
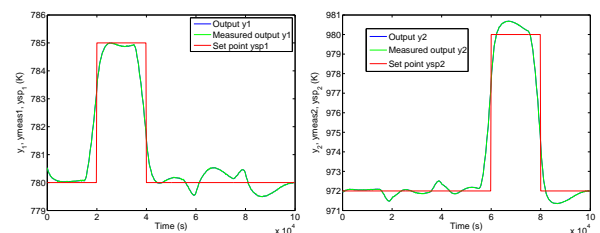
Figure 15: Observer Based Model Predictive Control with $H_p = 20$, $H_{p,low} = 1$, $\sigma_y = 0.01$. Left: Riser temperature (K). Right: Regenerator temperature (K).
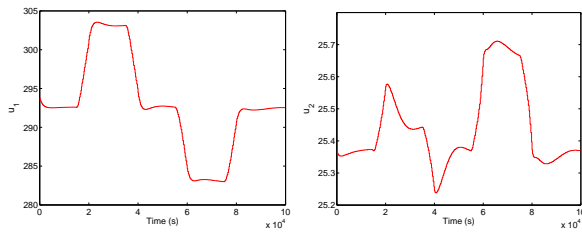
Figure 16: Observer Based Model Predictive Control with $H_p = 20$, $H_{p,low} = 1$, $\sigma_y = 0.01$. Left: Catalyst flow rate (kg/s). Right: Air flow rate (kg/s).

OBMPC with $\sigma_y = 0.5$

When a realistic noise of standard deviation $\sigma_y = 0.5$ is added to simulate noise on temperature measurement, the tendencies observed in the absence of measurement noise are preserved, i.e. outputs (Figure 17) follow very well the set points and variations of the manipulated inputs are smooth (Figure 18). Compared to all the previous MPC strategies, OBMPC presents the best performance. Obviously, the strong interactions present in the plant are better handled than by DMC-type algorithms, as claimed by [62].
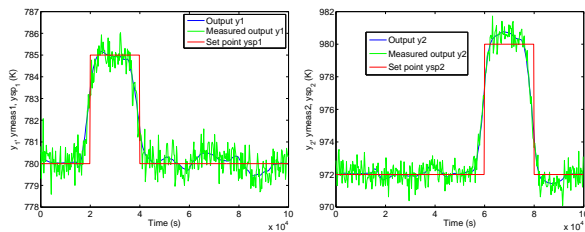
Figure 17: Observer Based Model Predictive Control with $H_p = 20$, $H_{p,low} = 1$, $\sigma_y = 0.5$. Left: Riser temperature (K). Right: Regenerator temperature (K).
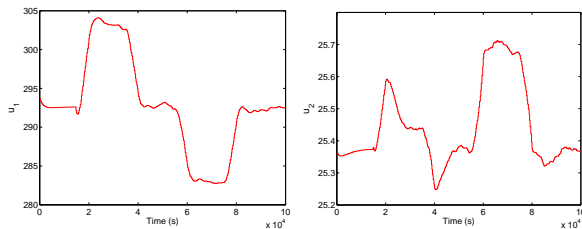
Figure 18: Observer Based Model Predictive Control with $H_p = 20$, $H_{p,low} = 1$, $\sigma_y = 0.5$. Left: Catalyst flow rate (kg/s). Right: Air flow rate (kg/s).

4. Conclusion

A nonlinear model of a Fluidized Catalytic Cracker (FCC) is presented. It can serve as a benchmark for Model Predictive Control (MPC) as several multivariable control structures can be tested. Furthermore, it presents important nonlinearities, interactions between the outputs and the outputs display an inverse response behaviour with respect to the catalyst flow rate that is one of the manipulated inputs. Several MPC strategies are presented and tested on this FCC model, DMC with analytical solution, QDMC with quadratic optimization, linear MPC with a penalty function and nonlinear optimization, Nonlinear MPC with model integration over the prediction horizon and nonlinear optimization, Observer Based MPC with a state-space model, an observer and quadratic optimization. The best performance was obtained by OBMPC, but QDMC and MPC-penalty gave also very good results. The most difficult control strategy was Nonlinear MPC which was not easy to tune and is not suited for on-line control, at least under the presented form.

Hard constraints on the manipulated inputs and their moves and soft constraints on the controlled outputs could be added to this problem, however, for comparison purpose, it was judged not necessary to introduce them.

Acknowledgement

References

[1] A. A. Avidan and R. Shinnar. Development of catalytic cracking technology. a lesson in chemical reactor design. *Ind. Eng. Chem. Res.*, 29:931–942, 1990.

[2] C. I. C. Pinheiro, J. L. Fernandes, L. Domingues, A. J. S. Chambel, I. Graa, N. M. C. Oliveira, H. S. Cerqueira, and F. R. Ribeiro. Fluid catalytic cracking (FCC) process modeling, simulation, and control. *Ind. Eng. Chem. Res.*, 51:1–29, 2011.

[3] R. Sadeghbeigi. *Fluid Catalytic Cracking Handbook*. Butterworh-Heinemann, Woburn, MA, USA, second edition, 2000.

[4] E. E. Ali and S. S. E. H. Elnashaie. Nonlinear model predictive control of industrial type IV fluid catalytic cracking (FCC) units for maximum gasoline yield. *Ind. Eng. Chem. Res.*, 36:389–398, 1997.

[5] L. F. L. Moro and D. Odloak. Constrained multivariable control of fluid catalytic cracking converter. *J. Proc. Cont.*, 5:29–39, 1995.

[6] A. Arbel, Z. Huang, I. H. Rinard, R. Shinnar, and A. V. Sapre. Dynamic and control of fluidized catalytic crackers. 1. Modelling of the current generation of FCC's. *Ind. Eng. Chem. Res.*, 34:1228–1243, 1995.

[7] D. Ljungquist, S. Strand, and J. G. Balchen. Catalytic cracking models developed for predictive control purposes. *Modeling, Identification and Control*, 14(2):73–84, 1993.

[8] S. S. E. H. Elnashaie and S. S. Elshishini. Digital simulation of industrial fluid catalytic cracking units-IV dynamic behaviour. *Chem. Eng. Sci.*, 1993.

[9] I. S. Han and C. B. Chung. Dynamic modeling and simulation of a fluidized catalytic cracking process. Part I: Process modeling. *Chem. Eng. Sci.*, 56:1951–1971, 2001.

[10] I. S. Han and C. B. Chung. Dynamic modeling and simulation of a fluidized catalytic cracking process. Part II: Property estimation and simulation. *Chem. Eng. Sci.*, 56:1973–1990, 2001.

[11] R. C. Macfarlane, R. C. Reineman, J. F. Bartee, and C. Georgakis. Dynamic simulator for a model IV fluid catalytic cracking unit. *Comp. Chem. Engng.*, 17(3):275–300, 1993.

[12] H. Ali, S. Rohani, and J. P. Corriou. Modelling and control of a riser type fluid catalytic cracking (FCC) unit. *Trans. IChemE.*, 75, part A:401–412, 1997.

[13] X. Lan, C. Xu, G. Wang, L. Wu, and J. Gao. CFD modeling of gas solid flow and cracking reaction in two stage riser FCC reactors. *Chem. Engng. Sc.*, 64:3847–3858, 2009.

[14] D. Kunii and O. Levenspiel. *Fluidization Engineering*. Wiley, New York, 1969.

[15] A. F. Errazu, H. I. de Lasa, and F. Sarti. A fluidized bed catalytic cracking regenerator model grid effects. *Can. J. Chem. Engng.*, 57:191–197, 1979.

[16] S. S. E. H. Elnashaie and I. M. El-Hennawi. Multiplicity of the steady state in fluidized bed reactors-IV. fluid catalytic cracking (FCC). *Chem. Eng. Sci.*, 1979.

[17] S. S. E. H. Elnashaie and S. S. Elshishini. Digital simulation of industrial fluid catalytic cracking units: Bifurcation and its implications. *Chem. Eng. Sci.*, 1990.

[18] S. S. Elshishini and S. S. E. H. Elnashaie. Digital simulation of industrial fluid catalytic cracking units: bifurcation and its implications. *Chem. Eng. Sci.*, 1990.

[19] J. M. Arandes and H. I. de Lasa. Simulation and multiplicity of steady states in fluidized FCCUs. *Chem. Eng. Sci.*, 47(9–11):2535–2540, 1992.

[20] M. Hovd and S. Skogestad. Procedure for regulatory control structure selection with application to the FCC process. *AIChE J.*, 39(12):1938–1953, 1993.

[21] M. Hovd and S. Skogestad. Pairing criteria for decentralized control of unstable plants. *Ind. Eng. Chem. Res.*, 33:2134–2139, 1994.

[22] J. Alvarez-Ramirez, J. Valencia, and H. Puebla. Multivariable control configuration for composition regulation in a fluid catalytic cracking unit. *Chem. Eng. J.*, 99:187–201, 2004.

[23] A. Arbel, I.H. Rinard, and R. Shinnar. Dynamic and control of fluidized catalytic crackers. 3. Designing the control system: choice of manipulated and measured variables for partial control. *Ind. Eng. Chem. Res.*, 35:2215–2233, 1996.

[24] P. Grosdidier, A. Mason, A. Aitolahti, P. Heinonen, and V. Vanhamäki. FCC unit reactor-regenerator control. *Comp. Chem. Engng.*, 17(2):165–179, 1993.

[25] J. J. Monge and C. Georgakis. Multivariable control of catalytic cracking processes. *Chem. Eng. Comm.*, 61:197–225, 1987.

[26] R. C. McFarlane, R. C. Reinemann, J. F. Bartee, and C. Georgakis. Analysis of fluidized bed catalytic cracking regenerator models in an industrial scale unit. *Comp. Chem. Engng.*, 17:275–300, 1993.

[27] M. V. Cristea, S. P. Agachi, and V. Marinoiu. Simulation and model predictive control of a UOP fluid catalytic cracking unit. *Chem. Eng. Proc.*, 42(2):67–91, 2003.

[28] R. M. Ansari and M. O. Tadé. Constrained nonlinear multivariable control of a fluid catalytic cracking process. *J. Proc. Cont.*, 10:539–555, 1997.

[29] R. Aguilara, J. Gonzalez, J. Alvarez-Ramirez, and M. Barron. Control of a fluid catalytic cracking unit based on proportional-integral reduced observers. *Chem. Eng. J.*, 15:77–85, 1999.

[30] L. F. L. Moro, A. C. Zanin, and J. M. Pinto. A planning model for refinery diesel production. *Comp. Chem. Engng.*, 22:s1039–1042, 1998.

[31] C. Loeblein and J. D. Perkins. Structural design for on-line process optimization: II. Application to a simulated FCC. *AIChE J.*, 45(5):1030–1040, 2004.

[32] A. C. Zanin, M. T. Gouvea, and D. Odloak. Industrial implementation of a real time optimization strategy for maximizing production of LPG in a FCC unit. *Comp. Chem. Engng.*, 24:525–531, 2000.

[33] V.W. Weekman and D.M. Nace. Kinetics of catalytic cracking selectivity in fixed, moving and fluid bed reactors. *AIChE J.*, 16(3):397–404, 1970.

[34] L. S. Lee, Y. W. Chen, T. N. Huang, and W. Y. Pan. Four-lump kinetic model for fluid catalytic cracking process. *Can. J. Chem. Engng.*, 67:615–619, 1989.

[35] P. Malay. A Modified Integrated Dynamic Model of a Riser Type FCC Unit. Master's thesis, University of Saskatchewan, Saskatoon, Canada, 1998.

[36] J. Ancheyta-Juarez, F. Lopez-Isunza, and E. Aguilar-Rodriguez. 5-lump kinetic model for gas oil catalytic cracking. *Appl. Catal. A*, 177:227–237, 1999.

[37] J. L. Fernandes, J. J. Verstraete, C. I. C. Pinheiro, N. M. C. Oliveira, and F. R. Ribeiro. Dynamic modelling of an industrial R2R FCC unit. *Chem. Eng. Sci.*, 62:1184–1198, 2007.

[38] X. Ou-Guan, S. Hong-Ye, M. Sheng-Jing, and C. Jian. 7-lump kinetic model for residual oil catalytic cracking. *Journal of Zhejiang University, Science A*, 11(7):1932–1941, 2006.

[39] C. Chen, B. Yang, J. Yuan, Z. Wang, and L. Wang. Establishment and solution of eight-lump kinetic model for FCC gasoline secondary reaction using particle swarm optimization. *Fuel*, pages 2325–2332, 2007.

[40] H. L. Wang, G. Wang, D. C. Zhang, C. M. Xu, , and J. S. Gao. Eight-lump kinetic model for upgrading residue by carbon rejection in a fluidized-bed reactor. *Energy Fuels*, 26:4177–4188, 2012.

[41] Y. Hongjun, X. Chunming, G. Jinsen, L. Zhichang, and Y. Pinxiang. Nine lumped kinetic models of FCC gasoline under the aromatization reaction conditions. *Catalysis Communications*, 7:554–558, 2006.

[42] S. M. Jacob, B. Gross, S. E. Voltz, and V. W. Weekman. A lumping and reaction scheme for catalytic cracking. *AIChE J.*, 22(4):701–713, 1976.

[43] J. Li, Z. H. Luo, X. Y. Lan, C. M. Xu, and J. S. Gao. Numerical simulation of the turbulent gas-solid flow and reaction in a polydisperse FCC riser reactor. *Powder Technology*, 237:569–580, 2013.

[44] P. Guigon, J. F. Large, and M. A. Bergougnou. Application of the Kunii-Levenspiel model to a multistage baffled catalytic cracking regenerator. *Chem. Eng. J.*, 28:131–138, 1984.

[45] H. I. De Lasa, A. Errazu, E. Barreiro, and S. Solioz. Analysis of fluidized bed catalytic cracking regenerator models in an industrial scale unit. *Can. J. Chem. Eng.*, 59:549–553, 1981.

[46] L. L. Lee, S. W. Yu, C. T. Chen, and W. Y. Pan. Fluidized-bed catalyst cracking regenerator modelling and analysis. *Chem. Eng. J.*, 40:71–82, 1989.

[47] A. Corma and J. Martinez-Triguero. Kinetics of gas oil cracking and catalyst decay on SAPO-7 and USY molecular sieves. *App Catal*, 118:153–162, 1994.

[48] E. Lee and F. R. Groves. Mathematical model of the fluidized bed catalytic cracking plant. *Transacions of the Society for Computer Simulation*, 2(3):219–236, 1985.

[49] J. P. Corriou. *Méthodes numériques et optimisation - Théorie et pratique pour l'ingénieur*. Lavoisier, Tec. & Doc., Paris, 2010.

[50] C. W. Gear and L. R. Petzold. Ode methods for the solution of differential/algebraic systems. *SIAM J. Numer. Anal.*, 21(4):716–728, 1984.

[51] K. Schittkowski. NLPQL: A Fortran subroutine solving constrained nonlinear programming problems. *Ann. Oper. Res.*, 5:485–500, 1985.

[52] C. Zhu, R.H. Byrd, P. Lu, and J. Nocedal. L-BFGS-B: a limited memory FORTRAN code for solving bound constrained optimization problems. Technical report, NAM-11, EECS Department, Northwestern University, 1994.

[53] J. P. Corriou. *Commande des Procédés*. Lavoisier, Tec. & Doc., Paris, third edition, 2012.

[54] J. P. Corriou. *Process Control - Theory and Applications*. Springer, London, 2004.

[55] C. R. Cutler and B. L. Ramaker. Dynamic matrix control - a computer control algorithm. In *AIChE Annual Meeting*, Houston, Texas, 1979.

[56] C. E. Garcia and A. M. Morshedi. Quadratic programming solution of dynamic matrix control (QDMC). *Chem. Eng. Comm.*, 46:73–87, 1986.

[57] R. Soeterboek. *Predictive Control - A Unified Approach*. Prentice Hall, Englewood Cliffs, New Jersey, 1992.

[58] F. Allgöwer and A. Zheng, editors. *Nonlinear Model Predictive Control*. Birkhäuser, Basel, 2000.

[59] G. Gattu and E. Zafiriou. Nonlinear quadratic dynamic matrix control with state estimation. *Ind. Eng. Chem. Res.*, 31:1096–1104, 1992.

[60] G. Gattu and E. Zafiriou. Observer based nonlinear quadratic dynamic matrix control for state space and input/output models. *Can. J. Chem. Eng.*, 73:883–895, 1995.

[61] J. H. Lee, M. Morari, and C. E. Garcia. State-space interpretation of model predictive control. *Automatica*, 30:707–717, 1994.

[62] P. Lunström, J.H. Lee, M. Morari, and S. Skogestad. Limitations of dynamic matrix control. *Comp. Chem. Engng.*, 19(4):409–421, 1995.

[63] N.L. Ricker. Model predictive control with state estimation. *Ind. Eng. Chem. Res.*, 29:374–382, 1990.

[64] S. Li, K. Y. Lim, and D. G. Fisher. A state space formulation for model predictive control. *AIChE. J.*, 35(2):241–249, 1989.